Real topography, atomic relaxations, and short-range chemical interactions in atomic force microscopy: The case of the α-Sn/Si(111)-$(\sqrt{3}\times\sqrt{3})R30°$ surface

Yoshiaki Sugimoto,[1,*] Pablo Pou,[2] Óscar Custance,[1] Pavel Jelinek,[3] Seizo Morita,[1] Rubén Pérez,[2] and Masayuki Abe[1,4]
[1]*Graduate School of Engineering, Osaka University, 2-1 Yamada-Oka, 565-0871 Suita, Osaka, Japan*
[2]*Departamento de Física Teórica de la Materia Condensada, Universidad Autónoma de Madrid, 28049 Madrid, Spain*
[3]*Institute of Physics, Academy of Sciences of the Czech Republic, Cukrovarnicka 10, 1862 53, Prague, Czech Republic*
[4]*PRESTO, Japan Science and Technology Agency, Saitama 332-0012, Japan*
(Received 25 October 2005; revised manuscript received 18 January 2006; published 16 May 2006)

We have investigated the phases of the Sn/Si(111)-$(\sqrt{3}\times\sqrt{3})R30°$ surface below $\frac{1}{3}$ ML coverage at room temperature by means of atomic force microscopy (AFM) and density functional theory based first-principles calculations. By tuning the Sn concentration at the surface we have been able to discriminate between Sn and Si adatoms, and to assure that the AFM topography for the different phases resembles the one reported using scanning tunneling microscopy. In the mosaic and the intermediate phases, a dependence of the topographic height of the Si adatoms on the number of surrounding Sn adatoms has been identified. In the pure phase, however, variations in the measured height difference between the Sn adatoms and the substitutional Si defects, which are intrinsic to the AFM observation, are reported. Reliable room-temperature force spectroscopic measurements using the atom-tracking technique and first-principles calculations provide an explanation for these striking induced height variations on the pure phase in terms of both the different strength of the short-range chemical interaction and tip-induced atomic relaxations. Our results suggest that the corrugation measured with true atomic resolution AFM operated at low interaction forces and close to the onset of significant short-range chemical interactions provides direct access to the real structure of heterogeneous semiconductor surfaces.

DOI: 10.1103/PhysRevB.73.205329 PACS number(s): 68.35.Bs, 68.35.Rh, 68.37.Ps

I. INTRODUCTION

In the past few years, the $(\sqrt{3}\times\sqrt{3})R30°$ structures of Pb and Sn grown on Si(111) and Ge(111) have received a remarkable attention both theoretically and experimentally.[1,2] The main motivation behind such interest is the appearance of low temperature phase transitions on Pb/Ge(111),[3–5] Sn/Ge(111),[6] and Pb/Si(111) (Refs. 7 and 8) and the absence of them on Sn/Si(111).[9,10] While controversy has characterized the different explanations for the phase transition driving force in the first three of these isovalent systems,[3–5,10–16] the absence of a soft phonon in the case of Sn/Si(111) (Ref. 10) seems to explain the $(\sqrt{3}\times\sqrt{3})R30°$ structure observed even at very low temperatures.[9] The wealth of knowledge accumulated on these surfaces makes them a very suitable playground for studying the interrelations between the topographic signal, the short-range interaction forces, and atomic relaxations in heterogeneous semiconductor surfaces using atomic force microscopy (AFM).

The true atomic resolution AFM—a recently developed technique also known as the noncontact atomic force microscopy[17–19]—has become a powerful tool for atomic-level observations and studies of metallic,[20] semiconductor,[21–23] and insulating surfaces,[24,25] and, nowadays, the obtained resolution rivals—and in some cases even surpass[26,27]—the one achieved using scanning tunneling microscopy (STM). Recently, it has been even demonstrated the capability of AFM for the manipulation of single atoms[28–30] that allows even engineering nanostructures atom-by-atom at room temperature.[30] In this study, however, we take advantage of the ability of quantifying the short-range chemical interaction forces between the tip-apex and the surface atoms[31–38] for the interpretation of striking topographic observations that we have detected. The analysis of the force spectroscopic measurements and the comparison with first-principles calculations shed light on the relation between the observed topographic contrast and the real structure of the surface. This combined analysis provides a clear understanding of how topographic AFM measurements at closer tip-surface distances are affected by atomic relaxations and differences in the interaction strength between the tip apex and the atomic species at the surface, explaining the striking variations in the height difference between the Sn adatoms and the substitutional Si defects. More importantly, our results suggest that, at a variance with other scanning probe microscopies like STM—where the contrast is dominated by electronic structure effects and, thus, topographic measurements do not necessarily correspond with the real height difference between the surface atoms—when imaging heterogeneous semiconductor surfaces with the AFM just below the onset of significant short-range chemical interactions, the topography detected seems to closely reproduce the real atomic corrugation expected for the surface.

II. EXPERIMENTAL AND THEORETICAL METHODS

In this work we have used a room-temperature dynamic scanning force microscope (SFM) in ultrahigh vacuum (UHV) environment (base pressure $<1\times10^{-10}$ Torr) operated following the frequency modulation detection method[39] and constant cantilever oscillation amplitude (CA-FM-AFM). The tip-surface interaction force was indirectly de-

tected throughout the detuning from the first mechanical resonant frequency of the cantilever; this frequency shift (Δf) is the main observable in CA-FM-AFM.[39] Force spectroscopic measurements were obtained recording the Δf as a function of the tip-sample relative vertical displacement (Z) over selected atomic positions of the surface. To obtain reliable $\Delta f(Z)$ curves at room temperature the combination of the CA-FM-AFM and the atom-tracking technique was implemented.[37,40] During both topographic and spectroscopic measurements the tip-sample contact potential difference was compensated by applying the corresponding bias voltage. Data acquisition was performed using a commercial scanning probe microscope controller (*Dulcinea*, Nanotec, S. L., Madrid, Spain). Commercial Si cantilevers (NanoWorld AG, Neuchatel, Switzerland) were cleaned up in UHV by Ar ion sputtering. Sb-doped Si(111) single crystals were used as substrates. The Sn/Si(111)-$(\sqrt{3}\times\sqrt{3})R30°$ surface preparation protocol was as follows: after cleaning the Si(111) sample by direct current heating in the UHV environment and obtaining the Si(111)-(7×7) surface, Sn was evaporated at room temperature and then the sample was annealed at 650° for typically 2 min. By adjusting the initial amount of Sn evaporated on the Si(111)-(7×7), it is possible to tune between the different phases of this surface: approximately $\frac{1}{6}$ ML is required for the mosaic phase, and $\frac{1}{3}$ ML for the pure phase[41] [1 ML is defined as the number of atoms in the first layer of the Si(111) surface].

Understanding the quantum nature of the tip-sample interaction and predicting its evolution during the scanning process is not an easy task as it requires two different key ingredients: the detailed knowledge of the structure at a given tip-sample distance and quantum mechanical calculations of the electronic properties associated with this geometry. Addressing this complex problem with a fully converged first-principles description in terms of an extended orbital basis like plane waves would limit our calculations—due to the computational resources needed—to a simple geometry, while different complex configurations are needed in order to provide a reliable comparison between the calculated tip-sample interaction and the experimental data. An appropriate choice, which we follow in this paper, is to resort to local orbital density functional theory methods, especially those derived with the aim of computational efficiency like the FIREBALL code,[42–45] that offers a very favorable accuracy-efficiency balance if the atomiclike basis set is chosen carefully.

In FIREBALL, the valence wave functions are expanded in the FIREBALL orbitals,[42,45] a set of strictly localized pseudoatomic orbitals—they are exactly zero for distances larger than the cutoff radius (R_C). We have used a minimal basis that includes s and p orbitals for Sn and Si with the following cutoff radii: R_C (Si s orbital) =4.8 a.u., R_C (Si p orbital) =5.4 a.u., and R_C (Sn s and p orbitals) =5.5 a.u. This basis set yields a very good description of the bulk properties of both elements: in the case of Si, we have obtained for the bulk diamond structure a lattice parameter $A=5.46$ Å and a bulk modulus $B=105$ GPa (experiment: $A=5.43$ Å, $B=100$ GPa), while for Sn, we have calculated for the α-tin phase bulk structure a lattice parameter $A=6.48$ Å and a bulk modulus $B=49$ GPa (experiment: $A=6.49$ Å, $B=53$ GPa).

In our calculations, we have used a supercell approach to mimic the CA-FM-AFM experimental situation. In particular, to model the Sn/Si(111)-$(\sqrt{3}\times\sqrt{3})R30°$ surface we have considered a (6×6) periodic slab that includes six Si layers and hydrogen atoms saturating the bonds of the deeper Si layer [see Fig. 5(a)]. The last two layers of the slab, the deeper Si and passivated H layer, were kept fixed during the relaxation process. The chosen (6×6) periodicity, that naturally accommodates the $(\sqrt{3}\times\sqrt{3})R30°$ surface reconstruction, is large enough to avoid spurious artificial interactions arising from periodic images in neighboring cells. The real tip-apex termination has been modeled by a well-tested nanoasperity of ten Si atoms in a Si(111) bilayer bonding configuration with a single atom protruding towards the surface [Fig. 5(a)]. The atoms at the topmost part of the tip were fixed and saturated with hydrogen, and the Si atom at the tip-apex has a single dangling bond pointing perpendicular towards the surface. This relatively simple tip model has been successfully used for, among other results, the interpretation of the imaging mechanism of CA-FM-AFM on semiconductors[46,47] as well as predictions on atomic manipulation experiments using dynamic AFM.[48] Our supercell, including both tip and surface slab, contains 289 atoms. Only the Γ point was included in the sampling of the Brillouin zone. The tip-sample interaction energy has been determined in a stepwise, quasistatic manner by approaching the tip parallel to the surface. At each step the atoms in the slab and the tip were allowed to relax to their ground state configuration for that particular tip position, with convergence criteria for the total energy and forces of 10^{-6} eV and 0.05 eV/Å. The short-range force was calculated as a numerical derivative of the total energy vs distance function.

III. TOPOGRAPHIC OBSERVATIONS

The Sn/Si(111)-$(\sqrt{3}\times\sqrt{3})R30°$ ($R3$ in the following) surface is a two-dimensional binary alloy showing intriguing electronic properties.[9,41,49–56] At room temperature, this surface has several phases depending on the Sn coverage: a pure phase (also called α-phase),[41] a mosaic phase (also called γ-phase),[41] and an intermediate phase.[51,54,55] The surface of the pure phase is ideally composed of only Sn adatoms, and it appears for a $\frac{1}{3}$ ML of Sn coverage. The mosaic phase is ideally composed of a 50% of Sn adatoms and a 50% of Si adatoms, yielding a Sn coverage of $\frac{1}{6}$ ML. The Sn coverage of the intermediate phase ranks between these values. In all these phases, the bonding configuration of Sn and Si is very similar: each adatom is located on a T_4 position over the Si(111) surface with four valence electrons in a sp^3-like-hybridization and one dangling bond pointing outwards from the surface plane. In spite of this relative simple structure, the surface electronic picture is rather complicated and differs from one phase to another due to electronic correlations between the Sn and the Si adatoms.[49,55,56] Both experimental and theoretical investigations indicate that while the pure phase shows a metallic behavior, the mosaic phase displays a semiconductor tendency due to a charge-transfer effect from the Si to the Sn adatoms.[49]

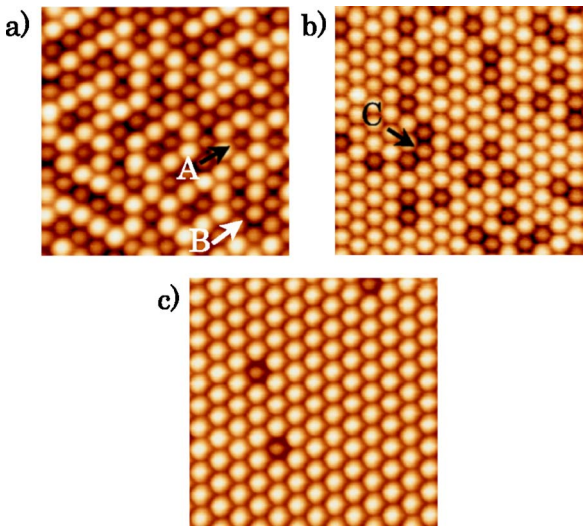

FIG. 1. (Color online) Topographic images of the Sn/Si(111) $-(\sqrt{3}\times\sqrt{3})R30°$ surface at different Sn coverage: (a) the mosaic phase, (b) the intermediate phase, and (c) the pure phase. Scan size is (8.5×8.5) nm^2. The arrows in (a) and (b) mark Si adatoms showing an unexpected topographic contrast due to variations in the number of the surrounding Sn adatoms. The acquisition parameters—the free-oscillation first mechanical resonant frequency (f_0), the cantilever stiffness (K), the cantilever oscillation amplitude (A), and the Δf set point—for each image were (a) $f_0=162\,167.6$ Hz, $K=30.5$ N/m, $A=19$ nm, and $\Delta f=-2.9$ Hz; (b) $f_0=161\,363.9$ Hz, $K=30.0$ N/m, $A=24$ nm, and $\Delta f=-5.1$ Hz; and (c) $f_0=162\,173.1$ Hz, $K=30.5$ N/m, $A=20$ nm, and $\Delta f=-4.7$ Hz, respectively.

In spite of this relatively complex electronic behavior, these surfaces are perfectly suitable for the observation with CA-FM-AFM. From theoretical studies it has been clarified that the imaging mechanism for atomic resolution using this technique on reactive semiconductor surfaces is attributed to the onset of a covalent bonding[46,47] between the outermost atom of the tip-apex and the atoms at the surface. It has been also demonstrated that the atoms on heterogeneous semiconductor surfaces occupying nonequivalent positions provide a different response to the interaction force with the SFM tip.[48,57] However, in the $R3$ surface, the Sn and Si adatoms are located at equivalent positions and, additionally, each atom has only one dangling bond for interacting with the tip.

Figure 1 shows topographic images of the mosaic (a), an intermediate (b), and the pure phase (c) of the $R3$ surface. We can distinguish two kinds of protrusions by the contrast difference in topography. Since the distances between them coincide with the geometry expected for the adatoms of the $R3$ structure, we have labeled them as bright and dim adatoms. An estimation of their proportion can be made by counting in large enough images typically containing more than a thousand of adatoms. In the images of the mosaic phase we have found a 47% of bright adatoms and a 53% of dim adatoms. A 98% (80%) of bright adatoms and a 2% (20%) of dim adatoms in the images of the pure (intermediate) phase have been, respectively, detected. Since the amount of bright adatoms on the surface increases by increasing the concentration of evaporated Sn, we can unambiguously identify the bright protrusions as Sn, and the dim ones as Si.

In a careful inspection of the topographic images of these surfaces, Si adatoms with different heights have been identified. In the mosaic phase, for example, the height of the adatom labeled as B—surrounded by five Si adatoms and only one Sn adatom—is $\sim$0.53 Å higher than that of the adatom labeled as A, which is surrounded by six Sn adatoms.[58] Similar effects also appear in the intermediate phase as it can be seen in Fig. 1(b): the height of the adatom labeled as C, surrounded by four Sn adatoms, is slightly higher than that of other Si adatoms surrounded by five or six Sn adatoms. This relation between the reduction in the Si adatom height when increasing the number of first neighboring Sn adatoms[59] has been attributed to a charge transfer from the Si adatoms to the Sn adatoms.[49,50,59] This charge transfer produces relaxations in the vertical position of the Si adatoms towards the substrate with respect to the rest of the Sn adatoms in the surface,[49,50] which retain their vertical positions almost independently on the number of neighboring Si adatoms.[59]

When exploring the pure phase using CA-FM-AFM, changes in the relative Sn-Si topographic height with a different origin have been identified. In this phase, a small concentration of Si atoms is usually found [Figs. 1(c) and 2(a)–2(c)], so they can be considered as substitutional defects at the perfect Sn surface.[50,52] For a low density of substitutional defects, these Si adatoms are usually equally surrounded by six Sn adatoms and, therefore, all of them show the same height difference—within the measurement error—with respect to the Sn adatoms. We have observed, however, that this height difference decreases upon a reduction in the tip-surface distance, i.e., when increasing the attractive interaction force. To show this behavior, we have obtained a series of images over the same surface area of the pure phase consecutively increasing the $|\Delta f|$ set point for each of them without any tip or surface change during the whole acquisition process. This series was measured within a tip-surface interaction force range that corresponds to tip-surface distances closer than the onset of significant short-range chemical interaction in order to stress the strong variations in the topography. Three representative images are shown in Figs. 2(a)–2(c).[60] The average height difference between the Sn adatoms and the Si substitutional defects are 0.37 ± 0.02 Å for Fig. 2(a) acquired at a normalized frequency shift value[61] of $\gamma=-6.3$ fN$\sqrt{m}$, 0.27 ± 0.03 Å for Fig. 2(b) ($\gamma=-7.3$ fN$\sqrt{m}$) and 0.05 ± 0.03 Å for Fig. 2(c) ($\gamma=-8.4$ fN$\sqrt{m}$). The dependence with the Δf set point value for the whole series [Fig. 2(d)] clearly shows that the Sn-Si height difference decreases, almost up to disappear, with increasing the $|\Delta f|$ set point, i.e., with decreasing the tip-surface distance.

When imaging this surface with STM,[9,50–53] a different topographic behavior is observed. In filled-states images these substitutional Si defects appear as a hole at the adatom position with the first neighboring Sn adatoms slightly brighter than the rest of the surface Sn adatoms.[49,50,52] In empty-states images the Si adatoms are generally visible (depending on the tunneling conditions) with slightly dim contrast, and the surrounding Sn adatoms appearance does not

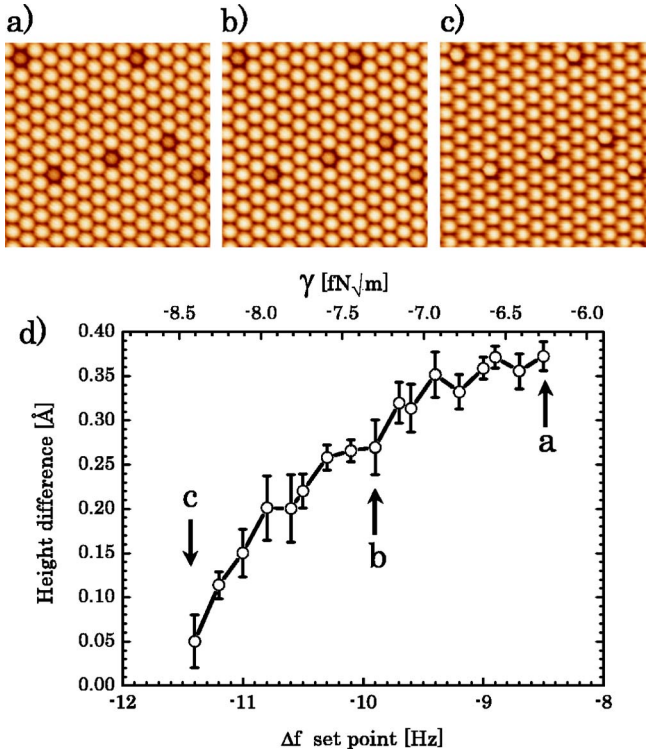

FIG. 2. (Color online) Topographic height variations of substitutional Si defects on the $\frac{1}{3}$ ML (pure phase) Sn/Si(111)$-(\sqrt{3}\times\sqrt{3})R3°$ surface when decreasing the tip-sample distance. (a)–(c) selected frames from a series of images (Ref. 60) showing the reduction of the topographic height on the Si adatoms when increasing the tip-surface interaction. Image dimensions are (8.5 $\times$8.5) nm^2. (d) Dependence of the Sn-Si topographic height difference with the Δf set point. The acquisition parameters were f_0 =162 285.8 Hz, K=30.5 N/m, and A=20 nm.

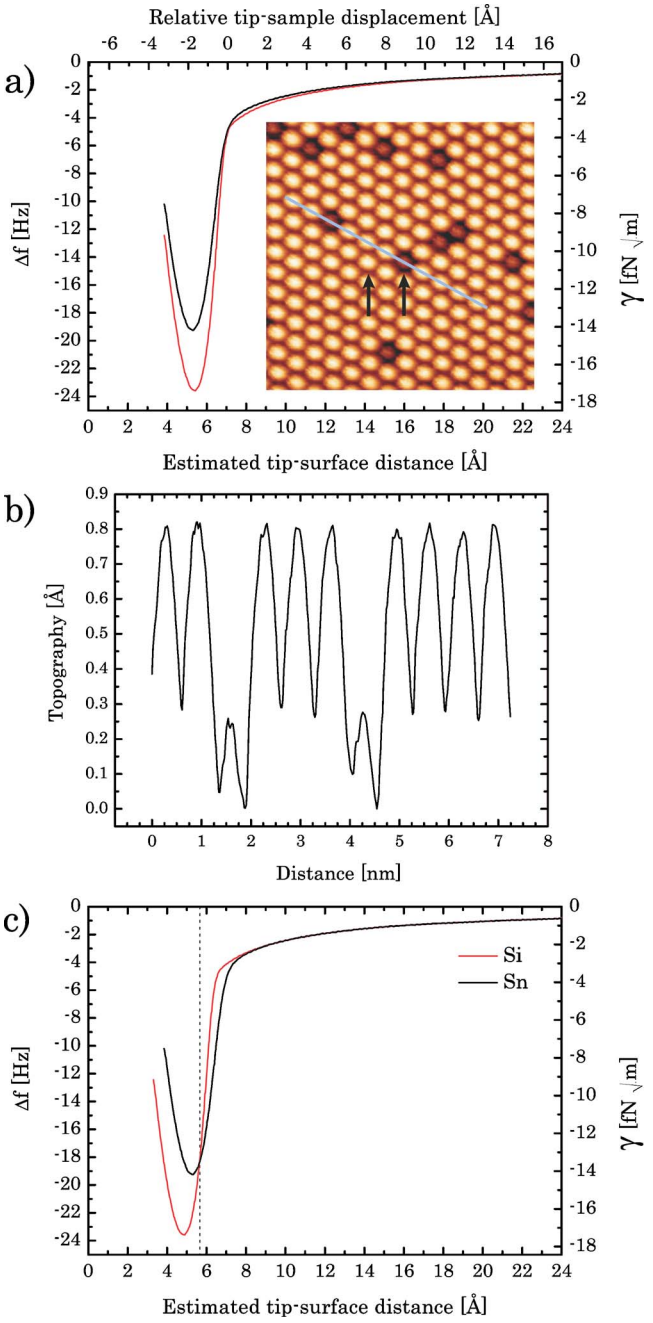

FIG. 3. (Color online) Room-temperature atomic force spectroscopic measurements. In (a) and (c) each of the displayed curves was obtained from the average of a hundred of equivalent $\Delta f(Z)$ curves measured over the Si and the Sn adatoms pointed in the inset image using the atom-tracking technique. In (c), the $\Delta f(Z)$ curve for the Si adatom has been shifted to take topographic effects during the acquisition into account. The dotted line indicates the crossing point between both curves. (b) Topographic profile highlighted in the image. The acquisition parameters were f_0=162 285.8 Hz, K =30.5 N/m, and A=25.9 nm. The set-point value for imaging and atom-tracking operation was Δf=−5.4 Hz. Image size is (8.5 $\times$8.5) nm^2.

differ too much from that of the other Sn adatoms at the surface.[49,50,52] Our CA-FM-AFM images resemble the STM empty-states images with the difference of a clear observation of the Si adatom slightly below the surface plane defined by the Sn adatoms. We should note that, while in STM electronic effects dominate over structural differences and the images map the local density of states of the surface, the atomically resolved topography in CA-FM-AFM reflects mainly the force associated with the covalent bond formation of the outermost tip-apex atom with the surface. In the low interaction regime, close to the onset of bond formation, this interaction decreases exponentially with the tip-surface distance. The fact that we observe a lower topography on the Si adatom for far enough tip-surface distances points to a permanent geometrical relaxation of the Si atom in the vertical direction towards the substrate. From first-principles calculations it has been reported that in the pure phase of the $R3$ surface the vertical position of the Si adatom should be near 0.5 Å lower than that of the Sn adatoms.[49,50] These predictions are in good agreement with the topographic difference we have detected at low interaction forces [Fig. 3(b)].

An intriguing fact is, however, the reduction of the Sn-Si topographic height difference when increasing the tip-surface attractive interaction force. This behavior suggests, *a priori*, two possible explanations: that there is a different chemical behavior between the Sn and the Si adatoms with the tip apex or, on the other hand, that the interaction with the SFM tip produces structural vertical distortions on the adatoms so

that a reduction of the height difference is finally obtained. More information for clarifying this matter can be provided by the analysis of site-specific force spectroscopic measurements.

IV. FORCE SPECTROSCOPIC RESULTS

In CA-FM-AFM experiments, it is possible to quantify the interaction force between the tip and the atoms at the surface by means of force spectroscopy.[31,37,40] In this kind of measurements the force is indirectly obtained from the variation of the Δf as a function of the tip-sample relative vertical displacement (Z) at specific atomic positions. Since these experiments were conducted at room temperature, the atom-tracking technique was applied for obtaining reliable $\Delta f(Z)$ curves.[37,40] First, using the positioning feedbacks of the atom tracking, the SFM tip was locked above the center of a Si adatom with a lateral precision better than ±0.1 Å;[37] then, after momentarily opening the atom-tracking feedback loops, a $\Delta f(Z)$ curve was acquired within 3 sec—in the experiments presented here the thermal drift velocity ranged from 0.25 to 1.34 Å/min—and afterwards the atom tracking was reactivated for continuing following the adatom. By repeating this procedure, a hundred of equivalent $\Delta f(Z)$ curves were obtained comprising the spectroscopic measurement over the Si adatom. After checking that neither the tip-apex nor the surface was modified during the acquisition process, the SFM tip was positioned on a Sn adatom and the same acquisition protocol was applied resulting in another hundred of $\Delta f(Z)$ curves measured over the Sn adatom. Again the absence of tip or surface modifications was assured by imaging the surface region afterwards. The very low dispersion between the $\Delta f(Z)$ curves of each series allows us to average them in a low-noise single $\Delta f(Z)$ curve.[37,40] The corresponding averaged $\Delta f(Z)$ curves for the Si and the Sn adatoms are shown in Fig. 3(a), and the measurements were respectively performed above the adatoms marked in the inset image.

In Fig. 3(a), the averaged $\Delta f(Z)$ curves are plotted as registered. These curves meet at $\Delta f=-5.4$ Hz, which was the set point value for the topographic feedback during both imaging [inset in Fig. 3(a)] and atom-tracking operations. In our implementation, the origin for the relative tip-sample vertical displacement in a $\Delta f(Z)$ curve acquisition corresponds to the separation that satisfies the topographic set point. When probing the Si adatom, the tip was, therefore, closer to the sample than in the Sn case. This effect is not taken into account in the plot shown in Fig. 3(a), and it manifests in the different tendency observed in the long-range contribution region. A fair comparison of these curves, as well as the further obtained interaction forces, requires the inclusion of this topography induced tip-height variation associated to the acquisition. Common values in the vertical displacement for both curves with respect to the surface plane are therefore obtained by shifting the Si curve by a distance that exactly matches the measured Sn-Si height difference at the given topographic Δf set point. From the image recorded after the spectroscopic acquisition [Fig. 3(a)] this distance corresponds to 0.54 Å [Fig. 3(b)]. The same curves after the shift are shown in Fig. 3(c): now both curves

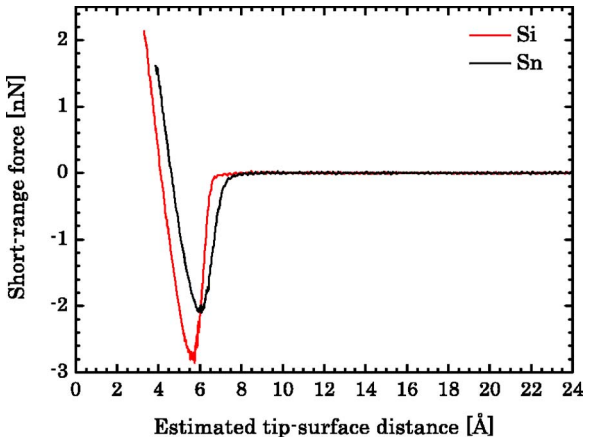

FIG. 4. (Color online) Short-range force associated with the $\Delta f(Z)$ curve shown in 3(c). Acquisition parameters are listed in the caption of Fig. 3.

are exactly the same up to reaching the region in which the short-range force contribution over the Sn adatom becomes dominant, reflecting the common long-range interaction.

An interesting feature in the curves of Fig. 3(c) is the new crossing point, which is highlighted by a dotted line. The behavior of the Δf curves is consistent with the observation of the Sn-Si topographic height reduction with increasing $|\Delta f|$ mentioned above [Fig. 2(d)]. According to Fig. 3(c), the difference in the vertical tip-sample distance over the adatoms at a fixed Δf set point should gradually decrease with increasing $|\Delta f|$ up to reaching the crossing point, in which both atom species would appear at the same height.[62]

From the averaged $\Delta f(Z)$ curves we can indirectly calculate the interaction force. In CA-FM-AFM experiments, it can be shown that the Δf is a weighted average of the tip-surface interaction force over one oscillation cycle.[61,63] The total interaction force can be obtained by the inversion of this relation in a nontrivial mathematical operation. Among the different inversion procedures available,[63–65] we have obtained a better performance using the method proposed by Sader and Jarvis.[65] The short-range interaction force can be obtained by subtracting the long-range contribution from the total force.[31,34,37] Since during the data acquisition the contact potential difference between tip and surface was compensated—minimizing the electrostatic force—the main long-range contribution comes from the van der Waals interaction. An appropriate fitting of the total force in the long-range region[66] to a Hamaker-like analytic model for the van der Waals interaction of a sphere over a plane[31] provides a good approximation to the characterization of the long-range contribution. Finally, the short-range interaction force is obtained by this fit subtraction from the total force curve.

The plot in Fig. 4 shows the corresponding short-range interaction force curves obtained from the averaged $\Delta f(Z)$ curves displayed in Fig. 3(c). The tip-surface distance in Figs. 3 and 4 is estimated by assuming the surface position at the divergence point for the fitting to the long-range contribution. These curves clearly show that the covalent bonding behavior of the Sn and the Si adatoms is different: the bonding force begins to be sensed over the Sn adatom at farther

tip-surface distances, and, additionally, the value of the attractive force minima is larger for the Si adatom. This behavior of the short-range forces over the Si and the Sn adatoms is independent of the tip-apex structure and composition—among the atomic species involved in these experiments—since different sets of force curves obtained over several measurement sessions with different tip apexes—some of them probably Sn contaminated—and calculations with Sn terminated tip models[67] always yield a stronger short-range interaction over the Si adatom.

V. DISCUSSION

The analysis of the different covalent bonding behavior of Sn and Si shown in Fig. 4 helps us understand the physical origin of the variation of the topographic Sn-Si height difference with the tip-surface distance (Fig. 2). According to these short-range force characteristics the Sn adatoms are imaged higher than the Si adatoms because the force sensed by the SFM tip is stronger above the Sn than that above the Si for an equivalent and large enough tip-surface separation. Therefore, the tip must get closer to the surface for detecting the necessary force at the Si adatom position for producing the required Δf set point. Upon approaching the tip to the surface, the Sn-Si topographic height difference should decrease as the bonding force sensed above the Si increases up to equal, and even exceed, the minimum force value sensed over the Sn; and accordingly, the tip must be approached less over the Si adatoms than before.

As it has been already suggested, the reduction in the Sn-Si topographic height difference could also be originated because of induced vertical relaxations due to the interaction with the tip apex. To experimentally demonstrate such an effect using the CA-FM-AFM, up to the date, is almost impracticable since when probing the atoms we are already perturbing a possible measurement. Thereby we have relied on first-principles calculations for identifying possible induced vertical relaxation effects.

Figure 5(b) shows a comparison of the forces obtained from calculations with the corresponding experimental short-range interaction (zooming in the plots of Fig. 4) at the Sn and Si positions. Here, the tip-sample distance is defined as the distance between the fixed layers in the tip and the slab. An arbitrary constant is subtracted in order to make the tip-sample distance equal to the normal distance between the tip apex and the Sn adatom when the tip and sample are far apart and there are no induced relaxations. With this definition, variations in the tip-surface distance are directly comparable to the relative displacements of the tip and sample, which are measured on the vertical piezo scale in the experiments. For the comparison, since the tip-surface distance in the calculation is well defined, the experimental curves have been shifted as a unit in the horizontal axis by 2.25 Å to align the minima for the Sn adatom. Although the agreement in the value at the force minima is excellent, the stiffness of the attractive and repulsive regions, i.e., the slope of the force curve in these two regimes, differs from those of the experimental curves due to the finite size of the tip,[31,37] atomic relaxations at the tip apex during the interaction with the surface may extend beyond an atomic bilayer. Recent simulations using larger, more complex, and therefore, more realistic tips have provided calculated force curves in a notable good agreement with experimental short-range forces in both

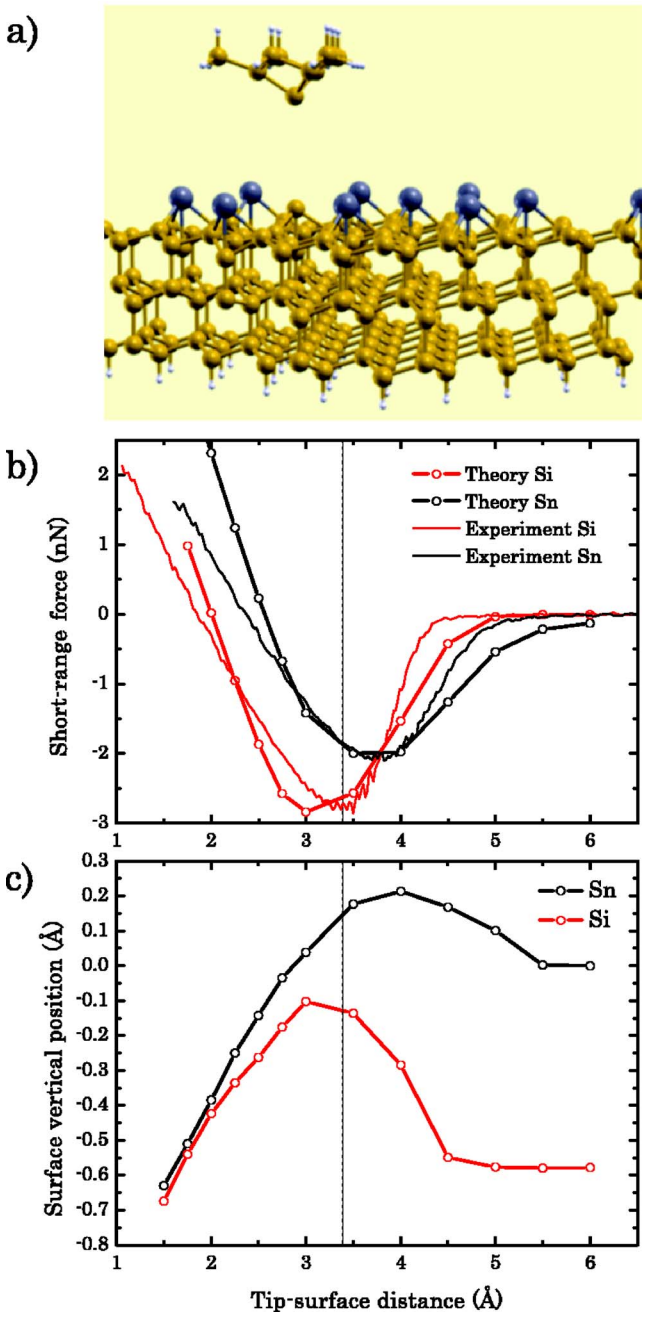

FIG. 5. (Color online) Results from first-principles calculations on the interaction of a Si tip apex with the Sn and the Si adatoms of the $Sn/Si(111)-\sqrt{3}\times\sqrt{3}R3°$ surface. (a) Tip and surface atomic models used in the calculations. (b) Comparison of the calculated covalent interaction forces with the experimental short-range forces displayed in Fig. 4. (c) Induced relaxations on the adatom vertical positions due to the interaction force as the tip approaches the surface. The dotted line marks the corresponding position of the crossing point between the $\Delta f(Z)$ curves displayed in Fig. 3(c). For a proper comparison with the theoretical curves, both the experimental force curves and the dotted line have been shifted as a unit in 2.25 Å towards the origin with respect to Figs. 3 and 4.

the value at the force minima and the stiffness of the attractive and repulsive regions.[38] In the case of Fig. 5(b), the excellent agreement between the experimental and calculated force values at the minima suggests that the tip-apex termination for this experiment could be in the form of a Si atom with a single dangling bond pointing perpendicular towards the surface plane.

The analysis of the adatom vertical displacements when approaching this tip model to the surface [Fig. 5(c)] clearly indicates that the attractive interaction with the tip produces a structural vertical distortion lifting the Si adatom up much more than the Sn adatom. Initially, at very low interaction forces, the Sn-Si height difference remains close to the value for the isolated surface.[68] Upon increasing the attractive interaction force both surface adatoms experience a vertical relaxation towards the tip, which is more prominent over the Si. The onset of the covalent bonding with the tip atom provides extra charge to the Si (with an initial charge deficiency due to a charge transfer to the neighboring Sn adatoms[49]) favoring a larger vertical displacement than over the Sn. At tip-surface distances closer than the position of the force minima, the surface atoms relax back towards the surface due to Pauli repulsion.

These results suggest that the CA-FM-AFM, in contrast to other scanning probe techniques, can provide a fairly direct access to the true structure of the surface. In principle, the measured height in the topographic images does not correspond with the real height differences between the surface atoms, as the topography measured in CA-FM-AFM is a complicated convolution of the total tip-sample interaction and the structure of the surface, which can be also affected by the interaction with the tip. Our comparison between theory and experiments shows that only when imaging at low interaction forces (and so, disturbing very weakly the surface structure), the registered corrugation seems to reproduce the real (theoretical) topography expected for a surface [Fig. 3(b)]. In the high interaction force regime, two new effects have to be taken into account: (a) The tip-surface interaction produces significant displacements of the surface atoms during every oscillation cycle and (b) differences in the intrinsic strength of the interaction due to the nature of the chemical species [that reflect in the different values for the force minima in Fig. 5(b)] start to dominate over the distance dependence. Under these conditions, the measured contrast cannot be related anymore to the geometry of the free surface. For example, at the position of the crossing point between the Sn and Si $\Delta f(Z)$ curves shown in Fig. 3(c), which is indicated in Fig. 5(c) with a vertical dotted line (in Fig. 5 the line position has been shifted with respect to Fig. 3 according to the shift in the force curves), the measured topographic height difference between Sn and Si atoms on the surface is nearly inexistent as it is shown in Figs. 2(c) and 2(d), but the calculation shows that the height difference between the adatoms at the closest tip-surface distance in each oscillation cycle should be close to 0.2–0.3 Å.

VI. SUMMARY

The $\frac{1}{3}$ ML Sn/Si(111)-$(\sqrt{3}\times\sqrt{3})R30°$ surface has been explored at room temperature by means of constant-amplitude frequency-modulation atomic force microscopy. Variations in the topographic height of the substitutional Si defects when imaging at close enough tip-surface distances have been detected. Reliable site-specific force spectroscopic measurements using the atom-tracking technique and first-principles calculations have demonstrated that the reduction of the Sn-Si topographic height difference when increasing the tip-surface interaction force is originated by a greater strength in the interaction force over the Si adatoms than over the Sn adatoms accompanied by tip-induced vertical relaxations of both adatoms. These induced relaxations are more intense over the Si adatom due to a charge transfer from the tip atom. Comparisons between the calculated and the measured topography suggest that, in contrast to other scanning probe techniques, when imaging heterogeneous semiconductor surfaces using true-atomic-resolution AFM in the absence of dissipation signal (Ref. 38), the profiles measured at low interaction forces can be associated with the real surface topography; imaging at high interaction forces, however, may reflect more the difference in the interaction strength between the tip and the atomic species at the surface.

ACKNOWLEDGMENTS

This material is based on work supported by the Handai Frontier Research Center, by the 21st century COE program, and by a Grant in Aid for Science Research and Special Coordination Funds from the Ministry of Education, Culture, Sports, Science and Technology of Japan. The work of P.P and R.P. was supported by the Ministerio de Ciencia y Tecnologia (Spain) under Grants No. MAT2002-01534 and No. MAT2005-01298, and by the VI Framework Programme of the European Union under the STREP project FORCETOOL (Project No. NMP4-CT-2004-013684). P. P. acknowledges the financial support by the Ministerio de Ciencia y Tecnologia (Spain) through the Juan de la Cierva Programme. The work of P.J. was supported by the MSMT under Grant No. 1K05020 and under the project HPC-EUROPA (Project No. RII3-CT-2003-506079). Part of these calculations has been performed at the Centro de Computacion Cientifica de la UAM. R.P., P.J., and P.P. thank J. Ortega for very useful discussions.

*Corresponding author. Email address: ysugimoto@ele.eng.osaka-u.ac.jp

[1] J. Ortega, R. Pérez, and F. Flores, J. Phys.: Condens. Matter **14**, 5979 (2002), and references therein.
[2] L. Petersen, Ismail, and E. W. Plummer, Prog. Surf. Sci. **71**, 1 (2002), and references therein.
[3] J. M. Carpinelli, H. H. Weitering, E. W. Plummer, and R. Stumpf, Nature (London) **381**, 398 (1996).
[4] J. Guo, J. Shi, and E. W. Plummer, Phys. Rev. Lett. **94**, 036105 (2005).
[5] I. Brihuega, O. Custance, M. M. Ugeda, N. Oyabu, S. Morita, and J. M. Gómez-Rodríguez, Phys. Rev. Lett. **95**, 206102 (2005a).
[6] J. M. Carpinelli, H. H. Weitering, M. Bartkowiak, R. Stumpf, and E. W. Plummer, Phys. Rev. Lett. **79**, 2859 (1997).
[7] O. Custance, J. M. Gómez-Rodríguez, A. M. Baró, L. Juré, P. Mallet, and J.-Y. Veuillen, Surf. Sci. **482–485**, 1399 (2001).
[8] I. Brihuega, O. Custance, R. Pérez, and J. M. Gómez-Rodríguez, Phys. Rev. Lett. **94**, 046101 (2005).
[9] H. Morikawa, I. Matsuda, and S. Hasegawa, Phys. Rev. B **65**, 201308(R) (2002).
[10] R. Pérez, J. Ortega, and F. Flores, Phys. Rev. Lett. **86**, 4891 (2001).
[11] A. Goldoni and S. Modesti, Phys. Rev. Lett. **79**, 3266 (1997).
[12] J. Avila, A. Mascaraque, E. G. Michel, M. C. Asensio, G. LeLay, J. Ortega, R. Pérez, and F. Flores, Phys. Rev. Lett. **82**, 442 (1999).
[13] A. V. Melechko, J. Braun, H. H. Weitering, and E. W. Plummer, Phys. Rev. Lett. **83**, 999 (1999).
[14] A. V. Melechko, J. Braun, H. H. Weitering, and E. W. Plummer, Phys. Rev. B **61**, 2235 (2000).
[15] D. Farias, W. Kamiński, J. Lobo, J. Ortega, E. Hulpke, R. Pérez, F. Flores, and E. G. Michel, Phys. Rev. Lett. **91**, 016103 (2003).
[16] R. Cortés, A. Tejeda, J. Lobo, C. Didiot, B. Kierren, D. Malterre, E. G. Michel, and A. Mascaraque, Phys. Rev. Lett. **96**, 126103 (2006).
[17] S. Morita, R. Wiesendanger, and E. Meyer, *Noncontact Atomic Force Microscopy*, NanoScience and Technology (Springer-Verlag, Berlin, 2002).
[18] R. García and R. Pérez, Surf. Sci. Rep. **47**, 197 (2002).
[19] F. J. Giessibl, Rev. Mod. Phys. **75**, 949 (2003).
[20] C. Loppacher, M. Bammerlin, M. Guggisberg, S. Schär, R. Bennewitz, A. Baratoff, E. Meyer, and H.-J. Güntherodt, Phys. Rev. B **62**, 16944 (2000).
[21] F. Giessible, Science **267**, 68 (1995).
[22] S. Kitamura and M. Iwatsuki, J. Phys. Soc. Jpn. **34**, L145 (1995).
[23] Y. Sugawara, M. Ohta, H. Ueyama, and S. Morita, Science **270**, 1646 (1995).
[24] C. Barth and M. Reichling, Nature (London) **414**, 54 (2003).
[25] C. Barth and C. R. Henry, Phys. Rev. Lett. **91**, 196102 (2003).
[26] T. Eguchi, Y. Fujikawa, K. Akiyama, T. An, M. Ono, T. Hashimoto, Y. Morikawa, K. Terakura, T. Sakurai, M. G. Lagally, and Y. Hasegawa, Phys. Rev. Lett. **93**, 266102 (2004).
[27] S. Hembacher, F. J. Giessibl, and J. Mannhart, Science **305**, 380 (2004).
[28] N. Oyabu, O. Custance, I. Yi, Y. Sugawara, and S. Morita, Phys. Rev. Lett. **90**, 176102 (2003).
[29] N. Oyabu, Y. Sugimoto, M. Abe, O. Custance, and S. Morita, Nanotechnology **16**, S112 (2005).
[30] Y. Sugimoto, M. Abe, S. Hirayama, N. Oyabu, O. Custance, and S. Morita, Nat. Mater. **4**, 156 (2005).
[31] M. A. Lantz, H. J. Hug, R. Hoffmann, P. J. A. van Schendel, P. Kappenberger, S. Martin, A. Baratoff, and H.-J. Güntherodt, Science **291**, 2580 (2001).
[32] R. Stomp, Y. Miyahara, S. Schaer, Q. Sun, H. Guo, P. Grütter, S. Studenikin, P. Poole, and A. Sachrajda, Phys. Rev. Lett. **94**, 056802 (2005).
[33] S. Hembacher, F. J. Giessibl, J. Mannhart, and C. F. Quate, Phys. Rev. Lett. **94**, 056101 (2005).
[34] R. Hoffmann, L. N. Kantorovich, A. Baratoff, H. J. Hug, and H.-J. Güntherodt, Phys. Rev. Lett. **92**, 146103 (2004).
[35] M. Ashino, A. Schwarz, T. Behnke, and R. Wiesendanger, Phys. Rev. Lett. **93**, 136101 (2004).
[36] H. Hölscher, S. M. Langkat, A. Schwarz, and R. Wiesendanger, Appl. Phys. Lett. **81**, 4428 (2002).
[37] M. Abe, Y. Sugimoto, O. Custance, and S. Morita, Appl. Phys. Lett. **87**, 173503 (2005).
[38] N. Oyabu, P. Pou, Y. Sugimoto, P. Jelinek, M. Abe, S. Morita, R. Pérez, and O. Custance, Phys. Rev. Lett. **96**, 106101 (2006).
[39] T. R. Albrecht, P. Grütter, D. Horne, and D. Rugar, J. Appl. Phys. **69**, 668 (1991).
[40] M. Abe, Y. Sugimoto, O. Custance, and S. Morita, Nanotechnology **16**, 3029 (2005).
[41] C. Törnevik, M. Göthelid, M. Hammar, U. O. Karlsson, N. G. Nilsson, S. A. Flodström, C. Wigren, and M. Östling, Surf. Sci. **314**, 179 (1994).
[42] O. F. Sankey and D. J. Niklewski, Phys. Rev. B **40**, 3979 (1989).
[43] A. A. Demkov, J. Ortega, O. F. Sankey, and M. P. Grumbach, Phys. Rev. B **52**, 1618 (1995).
[44] J. P. Lewis, K. R. Glaesemann, G. A. Voth, J. Fritsch, A. A. Demkov, J. Ortega, and O. F. Sankey, Phys. Rev. B **64**, 195103 (2001).
[45] P. Jelinek, H. Wang, J. P. Lewis, O. F. Sankey, and J. Ortega, Phys. Rev. B **71**, 235101 (2005).
[46] R. Pérez, M. C. Payne, I. Štich, and K. Terakura, Phys. Rev. Lett. **78**, 678 (1997).
[47] R. Pérez, I. Štich, M. C. Payne, and K. Terakura, Phys. Rev. B **58**, 10835 (1998).
[48] P. Dieska, I. Štich, and R. Pérez, Phys. Rev. Lett. **95**, 126103 (2005).
[49] A. Charrier, R. Pérez, F. Thibaudau, J.-M. Debever, J. Ortega, F. Flores, and J.-M. Themlin, Phys. Rev. B **64**, 115407 (2001).
[50] W. Kamiński, P. Jelinek, R. Pérez, F. Flores, and J. Ortega, Appl. Surf. Sci. **234**, 286 (2004).
[51] L. Ottaviano, B. Ressel, C. Di Teodoro, G. Profeta, S. Santucci, V. Chab, and K. C. Prince, Phys. Rev. B **67**, 045401 (2003).
[52] S. T. Jemander, N. Lin, H. M. Zhang, R. I. G. Uhrberg, and G. V. Hansson, Surf. Sci. **475**, 181 (2001).
[53] B. Ressel, C. D. Teodoro, G. Profeta, L. Ottaviano, V. Chab, and K. C. Prince, Surf. Sci. **562**, 128 (2004).
[54] H. M. Zhang, S. T. Jemander, N. Lin, G. V. Hansson, and R. I. G. Uhrberg, Surf. Sci. **531**, 21 (2003).
[55] J. Lobo, A. Tejeda, A. Mugarza, and E. G. Michel, Phys. Rev. B **68**, 235332 (2003).
[56] R. I. G. Uhrberg, H. M. Zhang, T. Balasubramanian, S. T. Jemander, N. Lin, and G. V. Hansson, Phys. Rev. B **62**, 8082 (2000).
[57] S. H. Ke, T. Uda, I. Štich, and K. Terakura, Phys. Rev. B **63**, 245323 (2001).
[58] The adatom classification into the two atomic species involved in this surface (Si or Sn) was performed by counting the topo-

graphic adatom height distribution for the image shown in Fig. 1(a) in a similar fashion as reported elsewhere (Ref. 59).

[59] Y. Sugimoto, M. Abe, K. Yoshimoto, O. Custance, I. Yi, and S. Morita, Appl. Surf. Sci. **241**, 23 (2005b).

[60] See EPAPS Document No. E-PRBMDO-73-078616 for a movie of the topographic images of this series. This document can be reached via a direct link in the online article's HTML reference section or via the EPAPS homepage (http://www.aip.org/pubservs/epaps.html).

[61] F. J. Giessibl, Phys. Rev. B **56**, 16010 (1997).

[62] The normalized frequency shift (γ) value at the crossing point in Fig. 3(b) is -13.5 fN$\cdot\sqrt{m}$. This value slightly differs from the one at which the height difference almost disappears in Fig. 2(c). This is because the acquisition of these data was performed using different tips at different measurement sessions. For a given γ set point, the topography and, therefore, the height difference between the adatoms could differ from one tip to another since it ultimately depends on the interaction with the tip apex, which may vary in structure and composition from one measurement session to another.

[63] U. Dürig, Appl. Phys. Lett. **76**, 1203 (2000).

[64] F. J. Giessibl, Appl. Phys. Lett. **78**, 123 (2001).

[65] J. E. Sader and S. P. Jarvis, Appl. Phys. Lett. **84**, 1801 (2004).

[66] In the absence of vacancies for the characterization of the long-range contribution (Ref. 31), we have assumed that the long-range region embraces from the free-oscillation region to the position at which the total force curve for the Sn starts deviating from that of the Si (Ref. 34).

[67] Y. Sugimoto, P. Pou, T. Namikawa, P. Jelinek, M. Abe, S. Morita, R. Pérez, and O. Custance (unpublished).

[68] Differences in the basis set and the convergence criteria used in the present calculations have yielded a Sn-Si height difference of 0.58 Å, slightly larger than the value of 0.50 Å obtained in previous theoretical calculations.